

## EFFECT OF THE MILKY WAY ON MAGELLANIC CLOUD STRUCTURE

MARTIN D. WEINBERG

Department of Physics &amp; Astronomy, University of Massachusetts, Amherst, MA 01003-4525, USA

*Draft version October 18, 2018*

## ABSTRACT

A combination of analytic models and n-body simulations implies that the structural evolution of the Large Magellanic Cloud (LMC) is dominated by its dynamical interaction with the Milky Way. Although expected at some level, the scope of the involvement has significant observational consequences. First, LMC disk orbits are torqued out of the disk plane, thickening the disk and populating a spheroid. The torque results from direct forcing by the Milky Way tide and, indirectly, from the drag between the LMC disk and its halo resulting from the induced precession of the LMC disk. The latter is a newly reported mechanism that can affect all satellite interactions. However, the overall torque can not isotropize the stellar orbits and their kinematics remains disk-like. Such a kinematic signature is observed for nearly all LMC populations. The extended disk distribution is predicted to increase the microlensing toward the LMC. Second, the disk's binding energy slowly decreases during this process, puffing up and priming the outer regions for subsequent tidal stripping. Because the tidally stripped debris will be spatially extended, the distribution of stripped stars is much more extended than the HI Magellanic Stream. This is consistent with upper limits to stellar densities in the gas stream and suggests a different strategy for detecting the stripped stars. And, finally, the mass loss over several LMC orbits is predicted by n-body simulation and the debris extends to tens of kiloparsecs from the tidal boundary. Although the overall space density of the stripped stars is low, possible existence of such intervening populations have been recently reported and may be detectable using 2MASS.

## 1. INTRODUCTION

The Magellanic Clouds are a natural laboratory for investigating the evolution of stellar populations in dynamically interacting systems. Their populations are well studied and provide a basis for standard candle and population evolution studies. In addition, a variety of dynamical studies and simulations exploit the Milky Way–Clouds–Magellanic Stream interaction to both infer its complex history and constrain Milky Way mass models (Fujimoto & Sofue 1976, Lin & Lynden-Bell 1977, Davies & Wright 1977, Lin & Lynden-Bell 1982, Murai & Fujimoto 1986, Lin et al. 1995; see Lin et al. for a thorough historical discussion). The link between chemical evolution and externally driven structural evolution is a hard problem, and to date, there has been little work devoted to a self-consistent dynamical picture of Cloud evolution. To this end, this paper focuses on one specific aspect—the dynamical interaction between the Milky Way and the Large Magellanic Cloud—and ignores the likelihood of a significant interaction with the Small Magellanic Cloud (SMC) in the past or the possibility that the SMC originated in a tidal disruption event. This simplified scenario by itself admits a rich set of interacting mechanisms.

Recent work by myself and others points out that time-dependent tidal forcing can have significant evolutionary consequences for globular clusters and dwarf or canni-

balized galaxies (Chernoff et al. 1986, Aguilar et al. 1988, Weinberg 1994c, Gnedin & Ostriker 1997, Murali & Weinberg 1997ab, Vesperini 1997, Weinberg 1997). The same physics applies to non-isotropic distributions such as disks or disks embedded in halos. For example, Sellwood et al. (1998) explored the importance of these resonant mechanisms to thickening host disks by dwarfs and excitation of bending waves. Weinberg (1998, Paper I) found that the resonant interaction between the Milky Way and LMC is sufficient to excite a warp and cause lopsided asymmetries, depending on the Galactic halo potential and LMC mass. In that work, the LMC was structurally fixed. Here, we turn the tables by structurally fixing the Milky Way and applying the same physics to LMC evolution.

It is straightforward to see that the magnitude of such a disturbance to the LMC is large. Either the subtended size of the LMC on the sky or the rotation curve combined with an estimate of the Milky Way mass enclosed in the LMC orbit leads to a tidal radius of approximately 11 kpc. At 5 kpc from the center, the ratio of the tidal force to the self force has only dropped to approximately 20% assuming a flat rotation curve, a significant perturbation. Although this ratio drops quickly further inward, the effect of the tidal force is amplified by a spectrum of resonances between the LMC–Milky Way orbital fre-

quencies and internal LMC orbital frequencies. Simultaneously, the LMC disk axis precesses due to the coupling with its orbit about the Galaxy. This induces an additional interaction between the LMC disk and halo. Altogether, these mechanisms result in enhanced angular momentum and energy transfer between the orbit and internal motions. They thicken the disk, populate the spheroid and drive mass loss. The latter mechanism has direct analogy to globular cluster evolution (see refs. cited above).

This paper explores this basic picture as follows. First, §2 summarizes the inference of the LMC orbit and mass needed to estimate the time-dependent tidal force. We will then explore the underlying dynamical interaction in several steps. Analytically, effectively irreversible changes in energy and angular momentum occur at resonances between the frequencies of the applied perturbation and the stellar orbital frequencies. First, I will describe the results of a restricted computation which sums the effect of all the resonances directly. This idealized model treats the evolution of a disk without self-gravity in a fixed halo potential (§3.1). We find that the disk is notably heated and thickened in several gigayears. Although the omission of self-gravity surely leads to an overestimate of the heating, the simple model serves to illustrate the potential importance of the underlying physical mechanisms.

This example is followed up in §3.2 with a full n-body simulation using the force algorithm described in Weinberg (1999). This code uses a basis expansion tailored to the density profile and is well-suited to following a slowly changing system. The collisionless evolution is gravitationally self-consistent with the caveat that the Galactic mass model and LMC orbit remains fixed. The n-body results substantiate the simple restricted example in §3.1, although the rate of disk thickening is smaller due to the self-gravity of the disk. Specifically, the simulations predict a thickening rate of 70 pc/Gyr at a roughly constant rate over the duration (about 4 Gyr). The tail of the torqued distribution populates the LMC halo region. At the same time, the energy input does work on the potential and causes overall expansion of the disk. This offsets the increase in velocity dispersion that might be observed from heating in a fixed potential; in fact, expansion wins and the velocity dispersion observed at a 45° inclination at one disk scale length is very slowly dropping.

These results lead to a number of interesting predictions and implications. First, the stellar component should be as extended as the halo. Moreover, this is done without isotropizing the distribution since a modest change in direction of the orbital plane (and therefore its angular momentum vector) is relatively easy. In fact, Olszewski et al. (1996) outline the evidence that nearly all components of the LMC have disk-like kinematics regardless of their extent. Second, the dark halo and the kinematically evolved and extended stellar component are preferentially stripped. The stripped material continues to orbit with the

LMC and slowly spread in phase. Because the stripped stars are not part of the disk, they do not lie along the HI-defined Magellanic Stream but rather in a much more diffuse distribution. In other words, this scenario does not suggest looking in the gas stream for the stars. Finally, a thickened bound stellar component in the LMC and an extended unbound cloud surrounding the LMC will increase the rate of self microlensing and we will estimate the effect in §4. A final discussion with implications for the LMC and satellite systems in general is presented in §5 followed by a summary of results in §6.

## 2. MASS, STRUCTURE AND ORBIT OF LMC

There have been a wide variety of LMC censuses, most of which treat the LMC as a galaxy and use the standard mass and mass density estimates: rotation curves, star counts, surface brightness profiles. Two relatively recent rotation curve studies, Meatheringham et al. (1988) and Schommer et al. (1992), estimate LMC masses of  $6 \times 10^9 M_\odot$  and  $1.5 \times 10^{10} M_\odot$ . Similar limits follow from carbon star studies by Kunkel et al. (1997b). The main difference between these determinations is not the value of  $V_c$  for the Cloud but the radial extent of the rotation curve. Alternatively, from the Milky Way's point of view, the LMC is similar to an oversized globular cluster. Its tidal radius is measurable and depends on both the Milky Way rotation curve and the LMC mass (and, weakly, its profile). A preliminary estimate of the tidally inferred LMC mass (Nikolaev & Weinberg 1998) yields  $2 \times 10^{10} M_\odot$  but is consistent with the Schommer et al. estimate. A brief description of this result is provided in the Appendix.

Recent estimates of the LMC space velocity from archival plate (Jones et al. 1994) and Hipparcos (Kroupa & Bastian 1997) proper motions both lead to consistent estimates of the LMC orbital plane. The procedure used here to estimate the orbit is described in Weinberg (1995). For the Milky Way halo, I choose a  $W_0 = 3$  King model (1966) with  $r_t = 200$  kpc and mass scaled to  $4 \times 10^{11} M_\odot$  (Kochanek 1996). The rotation curve due to the Galaxy, then, is approximately flat in the region of the LMC orbit. Together with a disk, the overall rotation curve is a plausible representation of the observed Milky Way. With this halo model, both the space velocities estimated by Jones et al. and Kroupa & Bastian yield a similar perigalacticon of 46 kpc with apogalacticons of 72 kpc and 120 kpc. For lack of motivation to favor one of these over the other, I adopt the mean apogalacticon.

## 3. MILKY WAY HEATING OF THE LMC

Paper I described the excitation of structure in the Milky Way halo due to non-local resonant excitation that occurs well inside the LMC's orbit. From the LMC's point of view, the Milky Way is in orbit about the LMC and the same dynamical coupling that raises wakes in the halo affects the LMC disk. This periodic forcing changes the

angular momenta of orbits at commensurate frequencies and adds energy to the disk. In the absence of commensurabilities, the tidal forcing would be adiabatically reversible and not lead to long-term evolution (e.g. Weinberg 1994a). This is the same physics that “heats” stellar orbits in globular clusters (Weinberg 1994c, Murali & Weinberg 1997a, Gnedin & Ostriker 1997). In the globular cluster case, however, one is primarily concerned with the work done by the external perturbation. In a disk, a change only in the orbital angular momentum vector, with little energy transfer, can change the disk morphology.

The first subsection below illustrates the evolution based on this dynamical mechanism. The calculation is straightforward in the idealized scenario of a spheroid-dominated potential and axisymmetry and without explicit disk self gravity. It predicts significant evolution on a gigayear time scale. Including disk self gravity will lengthen the time scale but nonetheless this relatively short time scale motivates the more complete n-body treatment in §3.2.

### 3.1. Solution of Boltzmann equation

To estimate the evolution, I present a solution of the time-dependent collisional Boltzmann equation for orbits in a fixed potential. The angular momenta of individual stars change during passage through resonances as the disk slowly evolves. The change in the conserved angular momenta depends on the direction that an orbit crosses a particular resonance (see Henrard 1982 for discussion). A galaxy will have different phase-space densities on either side of the resonance resulting in a net gain or loss for the passage. The net change in the phase-space distribution function, then, due to the resonant heating takes the form of a collisional Boltzmann equation where the right-hand-side collision term depends on the gradient of the phase-space distribution function (see Appendix for additional detail). For simplicity, we assume that the background gravitational potential is constant in time, dominated by the halo. The now linear partial differential equation may be solved by finite-difference on a three-dimensional grid (e.g.  $E, J, J_z$ ). The  $z$ -axis is perpendicular to the disk plane. The ratio of the  $z$ -axis angular momentum to the total angular momentum is the cosine of the orbital-plane inclination angle,  $\beta$ :  $\cos \beta = J_z/J$ . At every time step, the potential is recomputed and any phase space whose stars have apocenters larger than the tidal radius are deleted from the grid. Although, these weakly bound stars may linger near the tidal boundary for some time in reality (Lee & Ostriker 1987), this *one way* tidal boundary is easy to implement. A  $W_0 = 1.5$  King model was chosen to represent the LMC gravitational potential and approximately fits the rotation curve.

Figure 1 shows the cumulative distribution of mass above the disk plane as the system evolves,  $M(Z)$ . After approximately 1 Gyr, 1% of the disk mass has a height

larger than 6 kpc and 10% above 3 kpc. The thickening occurs from the outside in, appearing as a flared population that fills in at smaller radii with time. This leads to a very thick disk or flattened spheroid population.

Figure 2 shows the edge-on projected surface mass density. One sees that the tidal envelope is filled in a gigayear, and over longer time scales the disk scale height is increasing (cf. the  $10^{-1}$  contour in Fig. 1). This trend is more apparent in phase space: the orbits at low binding energy are heated first and those at successively higher binding energy as time goes on. This is clearly seen in the energy-orbital inclination ( $E-\cos \beta$ ) projection of the phase space distribution (Fig. 3): the high binding energy inclined orbits—the upper and lower left corners—are successively filled in with time.

Also worthy of note is that  $\log M(Z)$  is roughly linear with  $Z$  at times larger than 1 Gyr. This suggests an exponential profile which has been recently reported for the RR Lyrae distribution in the LMC halo (Kinman et al. 1991). The sharp roll over at the tidal radius is suggestive of the observed star-count profile but may be an artifact of the one-way tidal boundary.

### 3.2. N-body solution

The idealized semi-analytic model suggests that the LMC disk structure will change on a  $10^9$  year time scale, roughly an LMC orbital time. Without disk self gravity, the calculation in §3.1 is expected to overestimate the disk thickening due to resonant heating, although it may underestimate the thickening due to self-consistent readjustment to the external work. In this section, we examine the details of the evolution by n-body simulation. To limit the number of parameters and difficulty of the simulation, we ignore orbital decay.

#### 3.2.1. Force solver

In order to estimate the evolution on large scales over long time periods, we need to suppress small scale noise as much as possible and this need is satisfied by the biorthogonal expansion technique (e.g. Clutton-Brock 1972, 1973, Kalnajs 1976, Fridman & Polyachenko 1984, Hernquist & Ostriker 1992). The approach uses the eigenfunctions of the Laplacian to construct a complete set of orthogonal functions that satisfies the Poisson equation. The projection of the ensemble particle positions on each member of the orthogonal series yields a set of coefficients, similar to determining a potential from a charge distribution in electrostatics. These coefficients may then be used to describe the density, gravitational potential or force in the expansion code. The most efficient implementations use analytically derived recursion relations to generate the functions. The expansion converges quickly and is most efficient when the lowest order function is a good fit to the underlying equilibrium. However, most astronomical distributions do not match the available sets of

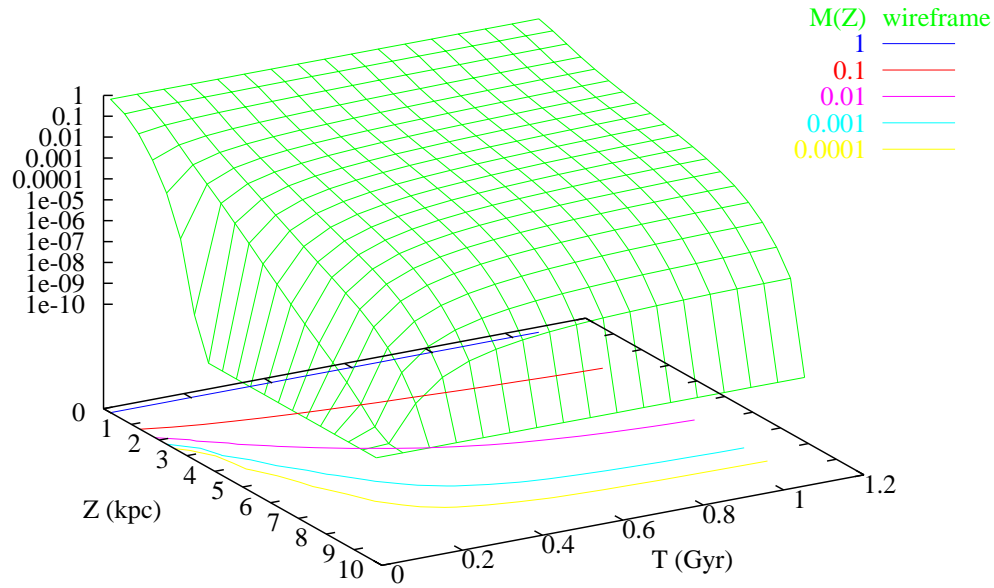


FIG. 1.— LMC disk heating by the Milky Way. Contours and wire frame show the cumulative distribution of stars at a height  $Z$  or larger. The curves show mass fractions  $1, 10^{-1}, 10^{-2}, 10^{-3}, 10^{-4}$  from bottom to top.

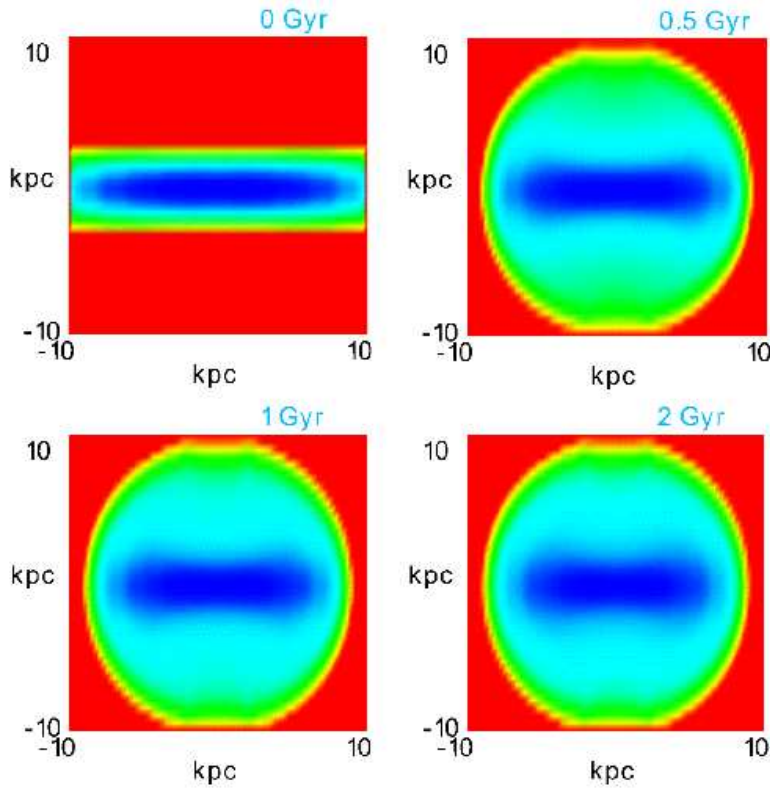


FIG. 2.— The projected surface density distribution for the edge on view of disk at four times shown in Fig. 1. The smooth color variation from red to green to blue reflects logarithmically change in projected surface density over six orders of magnitude from the peak.

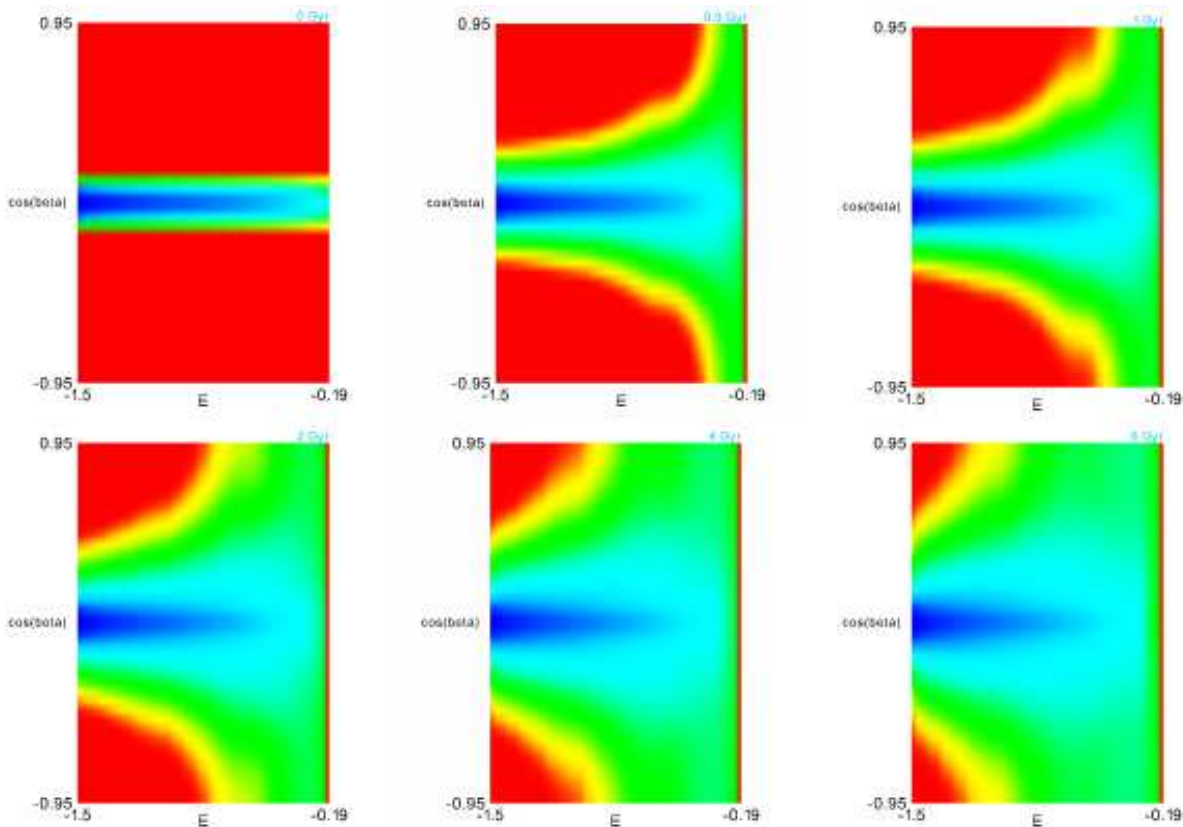


FIG. 3.— As in Fig. 2 but showing the phase space density in the  $E$  and  $\cos\beta \equiv J_z/J$  plane. NB: the evolution is both axisymmetric and symmetric around the midplane ( $\cos\beta = 0$ ).

special functions. The problem described in this paper motivated the algorithm developed in Weinberg (1999) which allows the adaptive construction of both spherical and three-dimensional cylindrical bases and this algorithm is used here.

Another advantage of this force solver is its ability to separately follow distinct kinematic components. Each component may be tied to a basis tailored to its geometry; this helps remove the bottleneck in simultaneously resolving multiple spatial scales. In particular, we can assign the halo particles to a spherical basis and the disk particles to a cylindrical basis. These are gravitationally coupled through the force evaluation. This procedure is easily extended. For example, a simulation which follows the response of the Milky Way halo simultaneously can be implemented by specifying an appropriate basis for the halo and following the halo response and its back-reaction on the LMC directly. This would increase the run time of simulations described here by only about 30%. These simulations will be performed in the next phase of this project.

Experimentation reveals that multiple expansion centers may introduce numerical feedback and excite oscillations. In principle, each component may be uncoupled as long as feedback is suppressed. For simulations here, the halo expansion center is tied to the disk center. The

force solver can easily resolve small offsets correctly so this is not a limitation for this application.

A parallel code with these features is implemented on a Linux-based cluster using MPI. Each node in the cluster has two processors; the algorithm was multi-threaded on each node to reduce the memory overhead. This allows the computation to be in core for all harmonic orders used here. The code performs load balancing but this is usually not required for the dedicated cluster. In practice, the average CPU load efficiency is approximately 90% for  $N = 10^5$  on 32 processors and improves for larger numbers of particles.

### 3.2.2. Parameters

The resolution of the force computation is set both by controlling the truncation in the series expansion and particle number. In the spherical case, one sets the maximum radial order,  $n_{max}$  and the maximum angular order  $l_{max}$ . In the cylindrical case, to start one has three indices corresponding the maximum radial order,  $n'_{max}$ , the maximum angular order  $m_{max}$ , and maximum vertical order. However, as described in Weinberg (1999), one can only adaptively choose the radial profile for the three-dimensional cylindrical set. For a particular spatial distribution and basis, the signal-to-noise ratio decreases with increasing order. We can empirically find new orthogonal functions to best represent the underlying

ing particle distribution to minimize noise. Here, this is done once based on the initial conditions (see Weinberg 1996, 1999 for details) and yields a two-dimensional indexed set,  $\mu_{max}, m_{max}$ . For problems here, we choose  $l_{max}, m_{max} = 2$  or  $4$ ,  $n_{max}, n'_{nmax} = 10$ , and  $\mu_{max} = 10$ . Within these limits, low signal-to-noise ratio components may be adaptively truncated. The evolution shows little difference to tests using larger series. The vertical expansion also requires specification of an outer boundary that is set to the initial tidal radius. Outside this radius, the force from the cylindrical component reverts to a monopole spherical force estimate. Finally, the time step is chosen to be approximately  $1/100$  of the shortest characteristic time scale (inner disk vertical motion) and the time evolution is followed using time-centered leap frog.

The total mass of the LMC is taken to be  $2 \times 10^{10} M_{\odot}$ , divided evenly between a halo and an exponential-sech<sup>2</sup> disk with  $a = 1.6$  kpc and  $h = 200$  pc (e.g. Wu 1994). The tidally truncated halo is represented by a King model with a core radius small enough to stabilize the disk against rapid bar formation. The potential of this halo profile includes a centrifugal potential during disk generation to better account for the non-inertial forces in the simulation. The LMC halo and orbit and disk generation by the quadratic programming technique is the same as that describe in Weinberg (1998). The simulations described here used  $N = 4 \times 10^5$  particles with  $1 \times 10^5$  in the disk and  $3 \times 10^5$  for the halo component. The large number of halo particles is needed to suppress the noise fluctuations which can disturb the disk. For the disk, the masses of the particles were scaled to produce a uniform number density distribution in cylindrical radius in order to better resolve the evolution of the outer disk. The halo particles have equal mass.

The external force on the LMC is expressed in the non-inertial frame of the center of mass of the LMC's orbit about the Milky Way:

$$\mathbf{f}_{tot}(\mathbf{x}) = \mathbf{f}_{self}(\mathbf{x}) + \mathbf{F}_{gal}(\mathbf{x} + \mathbf{R}(t)) - \mathbf{F}_{gal}(\mathbf{R}(t)) - 2\Omega(t) \times \mathbf{v} - \Omega(t) \times (\Omega(t) \times \mathbf{x}) - \dot{\Omega}(t) \times \mathbf{x}, \quad (1)$$

where  $\mathbf{x}$  is the position relative to the center of the LMC,  $\mathbf{R}(t)$  is the center of the LMC relative to the Milky Way,  $\mathbf{f}_{self}$  is the force of the LMC,  $\mathbf{F}_{gal}$  is the force of the Milky Way halo on the LMC and  $\Omega(t)$  is the time-dependent azimuthal frequency of the LMC about its orbit. Because the distance between the LMC tidal radius and the LMC galactocentric radius is not small, the Galactic component tidal force is evaluated by explicit difference rather than Taylor expansion of the underlying halo potential model.

The LMC orbit,  $\mathbf{R}(t)$ , is assumed to be fixed, that is, we ignore dynamical friction. This was done to reduce the dynamical complexity and number of parameters in favor of focusing on the internal evolution. Finally, because the

main goal is to look at the internal dynamical evolution of LMC, we ignore the effect of the SMC (e.g. Murai & Fujimoto 1980, Lin et al. 1995). Present day tidal effects are dominated by the Milky Way, although a close encounter with the SMC in past would also be a significant structure-changing event for the LMC.

### 3.2.3. Results

The galaxy is constructed to be in equilibrium in absence of the *time-dependent* tidal field. During the first  $6 \times 10^8$  years<sup>1</sup>), the system achieves a new approximate equilibrium. A slow ramp-up of the tidal terms in equation (1) yield larger initial transients. During the initial virialization phase, the disk responds strongly in its outer parts to the full non-inertial set of forces although the total mass involved is small. The inner disk oscillates as it phase mixes under the fully consistent self-potential and external galactic potential. Both effects have little effect on scale height. A simulation with the same initial conditions but with  $n_{max}$  increased by a factor of two shows the same behavior.

The LMC disk precesses under the torque from the Galaxy. Uncorrected, this would cause the expansion plane to drift away from the true disk plane defined by the instantaneous mean angular momentum. To follow this, the disk bodies are ranked by binding energy and the lowest 2% are used to determine the disk angular momentum vector and expansion center. To damp any numerical feedback, both the expansion plane and center are determined from a 100 time step running average.

This precession is shown in Figure 4 which shows the azimuth of the LMC disk's angular momentum axis in the original frame. The disk also nutates, as seen in Figure 5, because of the initial transient. The initial angle between the mean angular momentum vector perpendicular to the disk and the Galactic center is  $45^\circ$ . Although a non-nutating system might be achieved by iterating the initial angular momentum vector, there is little reason to assume this is closer to the natural state, so no corrections have been made.

At the same time, the LMC halo and disk have a mutual self-gravitating response that causes a slow  $m = 1$  oscillation of the disk density center. The existence of such weakly damped modes can be demonstrated analytically using the methods described by Weinberg (1994d). Because of these modes and the fact that mass and momentum loss in the Galactic tidal field is asymmetric, the potential expansion is chosen to track the density center. Although the force solver can handle this situation, the secular heating of disk increases. Tests without the tidal field confirm that this effect does not dominate or obscure the tidal heating (cf. Fig. 6).

<sup>1</sup>Time units here are based on a circular velocity of  $V_o = 200$  km/s at the Solar circle and peak rotation curve velocity in the LMC of  $V_{LMC} = 75$  km/s.

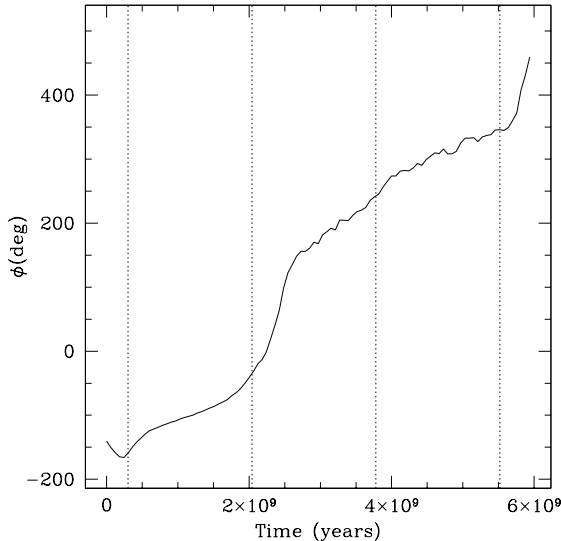


FIG. 4.— Change in azimuth of the precessing disk with time. The vertical dotted lines indicate perigalactica.

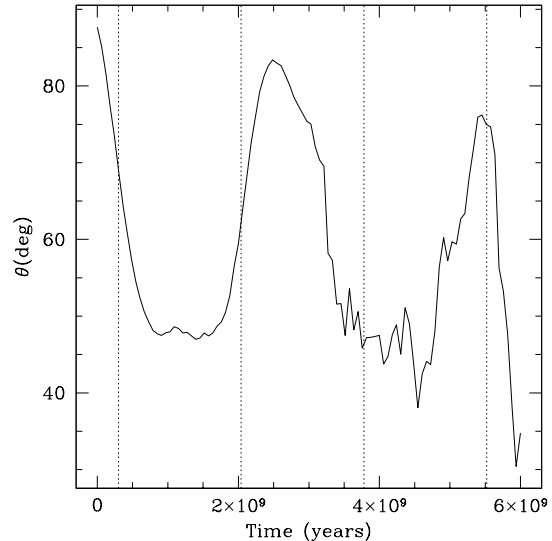


FIG. 5.— Colatitude of angular momentum axis of precessing disk with time. For comparison with Fig. 4, the vertical dotted lines indicate perigalactica.

The disk thickness is estimated from the density distribution in a column through the LMC at a radius of a disk scale length. The disk plane is inferred by the same method used to orient the force expansion (see §3.2). The line of sight inclination is chosen to be  $45^\circ$  and azimuthally averaged at one LMC disk scale length. The line of sight quantities are computed by selecting tracers in a pencil along the line of sight and estimating the one-dimensional density distribution using optimal kernel smoothing (Silverman 1986). The quantity  $\sigma_d$  denotes the half width corresponding to the mass enclosed within one Gaussian standard deviation. To convert to scale height  $h$  of the equivalent isothermal slab, an explicit evaluation determines that  $\sigma_d \approx 1.8h$ . With a  $45^\circ$  inclination, this is  $\sigma_d \approx 2.6h$ . The variance of the velocity distribution of stars along the line of sight is denoted  $\sigma_v^2$ .

Figure 6 shows  $h$  and  $\sigma_v$ . There are two clear trends: 1) the thickness of the disk increases; and 2) the velocity dispersion very slowly *decreases*. The slope, shown as a straight solid line in Figure 6, is  $70 \text{ pc/Gyr}$ . The evolved n-body disk has an approximately exponential profile, as also predicted by the semi-analytic computation. The linear increase in  $h$  with time is predicted by the underlying resonance theory and is a natural consequence of secular evolution.

The decrease in velocity dispersion seems counterintuitive at first glance but is often seen in globular cluster evolution. In a fixed gravitational potential, the heating would go into kinetic energy. However, the work done on the *self-gravitating* disk decreases the depth of the potential well and, by the virial theorem, also decreases the kinetic energy. The relative velocity dispersion tends to

increase owing to the increased orbital eccentricity and a larger projection of the velocity along the line of sight caused by increasing orbital inclination. However this is not enough to offset the overall decrease in kinetic energy and the magnitude of the dispersion decreases.

In summary, the effect of the heating is significant although not as dramatic as in the analytic computation that ignores the disk’s self gravity.

Figure 7 describes the mass loss as a function of time. Mass beyond the LMC tidal radius is assumed to be lost. Loss of dark halo material, disk stars and total are shown separately with the orbital pericenters indicated as vertical dotted lines. Roughly 10% of the halo and 3% of the disk is lost by  $T = 6 \text{ Gyr}$ . The halo material is lost episodically, with the peak loss just past every pericenter. The disk stars are lost at a roughly steady rate. A total mass of  $1.4 \times 10^9 M_\odot$  or 7% of the original mass is lost by  $T = 6 \text{ Gyr}$ . The spatial distribution of the LMC disk at this point is shown in Figure 8 in both edge-on and face-on projection. The colors here range from blue to red, orange, yellow and finally white as the mass density increases logarithmically. The outlying stellar spheroid that has been heated out of the disk is fairly tenuous and the edge-on disk is thinner than it appears. Figure 9 highlights the distribution of lost mass for both stars and halo material. In this figure, the lowest densities are shown as white. Recall, the relative number of points at different radii in these plots do not trace mass; the lower binding energies are preferentially represented as described in §3.2.2 in order to better resolve the mass loss.

### 3.3. Location of stripped mass

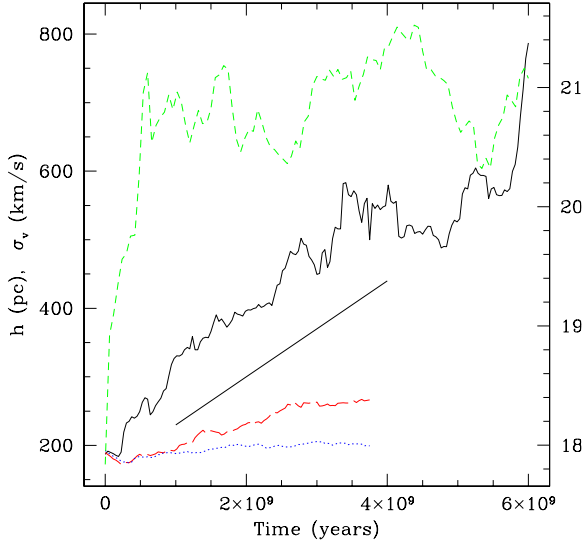


FIG. 6.— The scale height of the density distribution,  $h$  (left-hand axis: solid, long dash, dotted) and the root variance of the velocity distribution,  $\sigma_v$  (right-hand axis: upper dashed curve) for a line-of-sight inclined  $45^\circ$  to the LMC disk. The scale height of the LMC disk increases at a rate of  $70 \text{ pc/Gyr}$  (solid segment). The dotted and long-dashed curves show the secular evolution in absence of the Galactic tidal field for  $m = 0$  terms only and all terms, respectively. The velocity dispersion is nearly constant (note the small range in velocity) but decreases slowly on average after virialization.

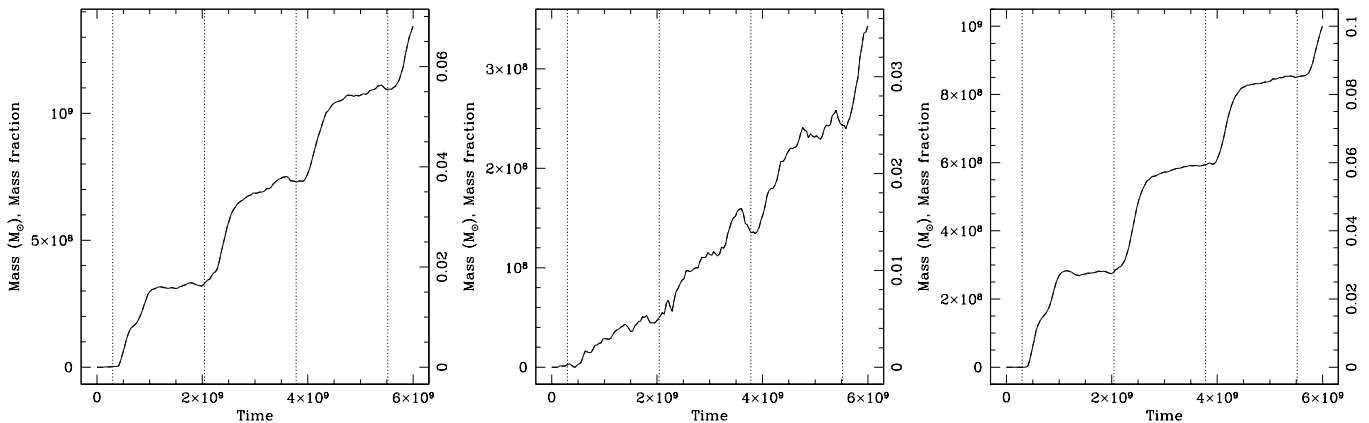


FIG. 7.— Mass loss as a function of time for total mass (left), LMC disk (center), and LMC halo (right). In each panel, the left axis describes mass in solar masses and the right describes mass fraction. The vertical dotted lines indicate perigalactica.

There have been a number of searches for stars associated with the observed gaseous Magellanic Stream (Sanduleak 1980, Recillas-Crus 1982, Brueck & Hawkins 1983, Kunkel et al. 1997a, Guhathakurta & Reitzel 1998). All but one of these studies target the HI distribution. Kunkel et al. study carbon stars in the outskirts of the LMC.

This paper suggests that the stellar debris has a different distribution than the gaseous stream. Tidal heating slowly advects the orbits to both high inclination and radius before they are lost to the Galactic potential. The stripped distribution, then, has a larger velocity dispersion than the kinematically cold disk component and is not collimated on the sky. This debris should not be expected to track

the stripped gas, which can dissipate and interact with the Galactic halo gas. A simulation that investigates this same scenario but includes gas dynamics is in preparation.

After three orbits, the LMC is surrounded by stripped material (cf. Fig. 10). Logarithmic contours and color coding highlight the low-density distribution. Note the low-level plateau of material surrounding the bound LMC. Figure 11 shows the location of the predicted stream in Galactic coordinates with logarithmic contour levels of projected mass density<sup>2</sup>. The stellar ejecta would spread along a great circle across the sky if viewed from the Galactic center. The low star count density predicted here, a few stars per square arc minute, is probably too low

<sup>2</sup>Figures 10 and 11 were made by kernel smoothing the n-body distribution onto a rectangular grid. In the latter case, the grid is first constructed in  $l$  and  $\cos b$  and rendered using an equal-area Hammer-Aitoff mapping. Unfortunately, the distortion due to the mapped bin shape is visible especially at the poles but the basic features are clear.



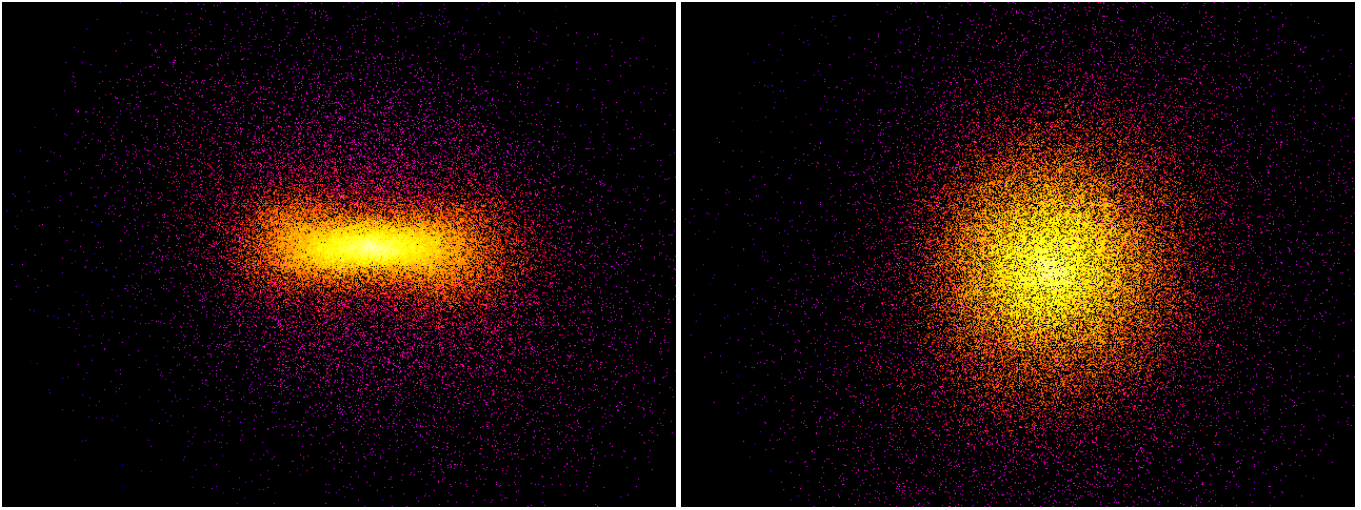


FIG. 8.— Edge-on (left) and face-on (right) views of the LMC disk after about 5 Gyr. The points are color coded to indicate mass density on a logarithmic scale from blue to yellow. The distance top to bottom is approximately 20 kpc.

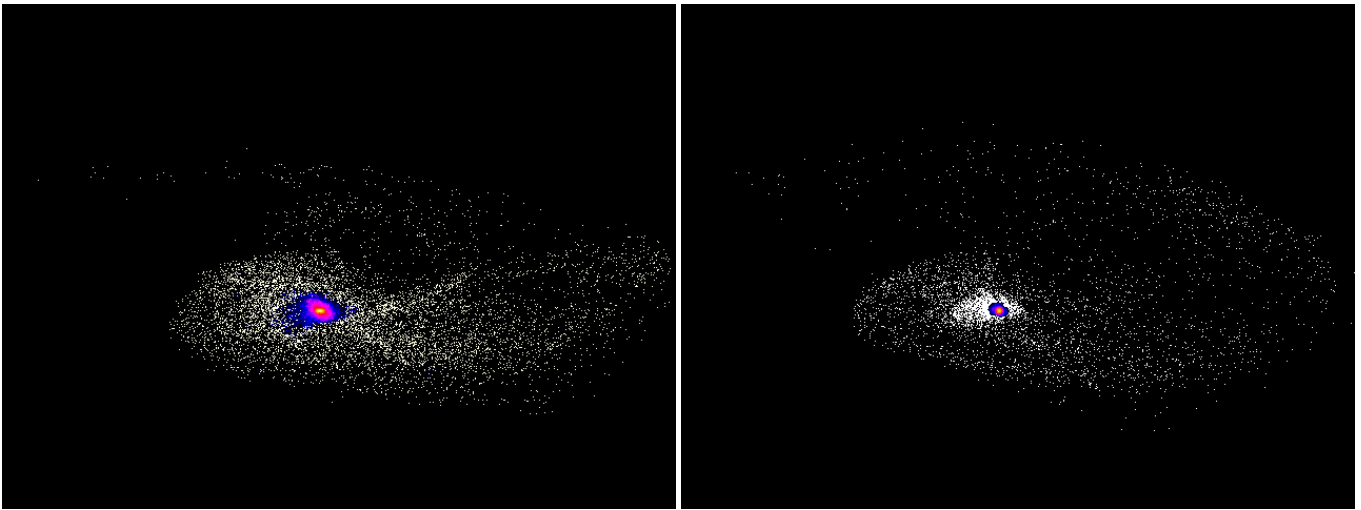


FIG. 9.— Large-scale views of evolved LMC, highlighting the low-density ejected material (white). The sharp edge is caustic due to stars lost at a previous perigalacticon. The distance top to bottom is approximately 50 kpc. The radius of the well-defined disk is approximately 10 kpc.

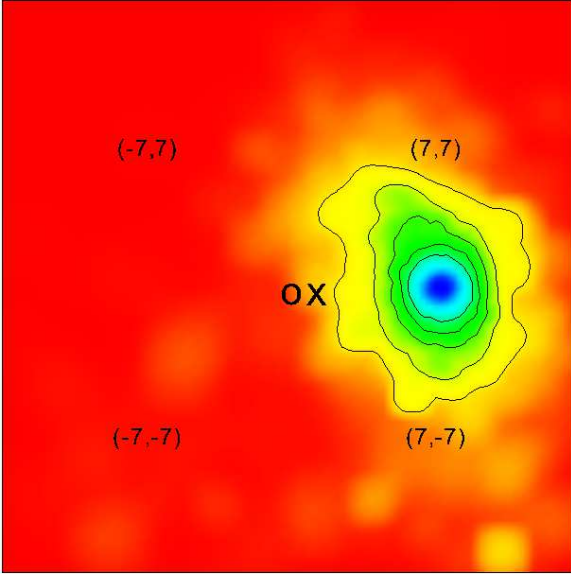


FIG. 10.— The projected stellar density perpendicular to the orbital plane. The Cloud is near pericenter and moving in the  $\hat{y}$  direction. The five contours are spaced logarithmically and correspond to  $1.5 \times 10^{-3} M_{\odot}/\text{pc}^2$  to  $1.5 \times 10^1 M_{\odot}/\text{pc}^2$ . Each unit of length in the simulation is 7 kpc; the points  $(\pm 7, \pm 7)$  are labelled. To provide a sense of scale, the ‘O’ and ‘X’ denote the Galactic center and an offset of 8 kpc, respectively.

to have been observed in small-area fields. For example, the limit of Guhathakurta & Reitzel (1998), based on deep photometry centered on the MSIV gas clump, is near but above the predicted projected stellar mass density in debris stars. However, the stripped material along the LMC orbit but still outside the LMC should be detectable by filtering a large-area survey along the predicted great circle. Such an analysis will be straightforward with a full-sky survey such as 2MASS. The carbon stars observed by Kunkel et al. (1997) in the outskirts of the LMC may be evidence for stellar debris near but outside the Cloud.

Comparing both Figures 10 and 11, it is clear that the distribution of stripped stars on the sky are likely to have a large spread in distance. Of particular interest is the extension in front of the LMC which may be a possible explanation for the observed intervening stellar population toward the LMC reported by Zaritsky & Lin (1997).

#### 4. MICROLENSING

An extended LMC stellar distribution, both bound and unbound, can enhance the microlensing optical depth caused by self-lensing. We can calculate the optical depth due to microlensing by using the estimated density distribution from the n-body simulation (see Appendix for details). We use the same Galactic halo model adopted by the MACHO collaboration for consistency (e.g. Alcock et al. 1997):

$$\rho_H = 0.0079 \frac{R_0^2 + a^2}{r^2 + a^2} M_{\odot}/\text{pc}^3, \quad (2)$$

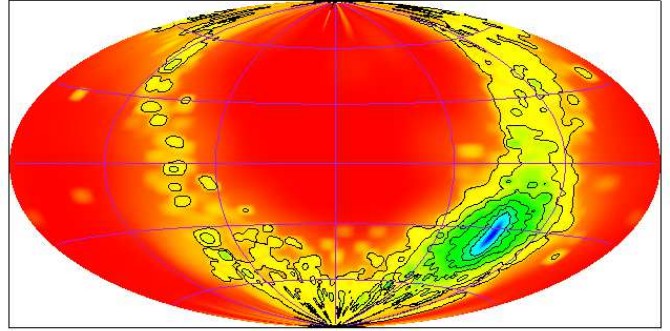


FIG. 11.— The projected stellar density on the sky in Aitoff projection. The five contours are spaced logarithmically and correspond to  $2 \times 10^1$  to  $2 \times 10^5$  solar masses per square arc minute. The simulation is shown with the LMC close to its current position.

where  $r$  is the Galactocentric radius,  $R_0 = 8.5 \text{ kpc}$  is the Galactocentric distance of the Sun and  $a \approx 5 \text{ kpc}$  is the core radius.

The optical depth averaged along the line-of-sight is given by

$$\tau = \int_0^{\infty} \tau(D_s) p(D_s) dD_s \left[ \int_0^{\infty} p(D_s) dD_s \right]^{-1}, \quad (3)$$

where

$$\tau(D_s) = \frac{4\pi G}{c^2} \int_0^{D_s} \rho_d(D_d) \frac{D_d(D_s - D_d)}{D_s} dD_d \quad (4)$$

is the optical depth due to sources at a distance  $D_s$ ,  $\rho_d$  and  $\rho_s$  are the lens and source densities respectively, and

$$p(D_s) dD_s = C \rho_s(D_s) D_s^{2+2\beta} dD_s \quad (5)$$

(Kiraga & Paczyński 1994) is the probability of finding a source in the interval  $[D_s, D_s + dD_s]$ . We take  $\beta = -1$ , consistent with a fit to the Bahcall-Soneira model (1980).

For these simulation-based estimates, the LMC location is chosen at a point in its orbit that matches its present position. Unfortunately, this does not guarantee that the orientation of the disk in the simulation corresponds to the one observed. Rather than perform expensive iterations, the coordinates are transformed to the observed true orientation. The line-of-sight density distribution is computed using the kernel smoothing procedure described in §3.2.3.

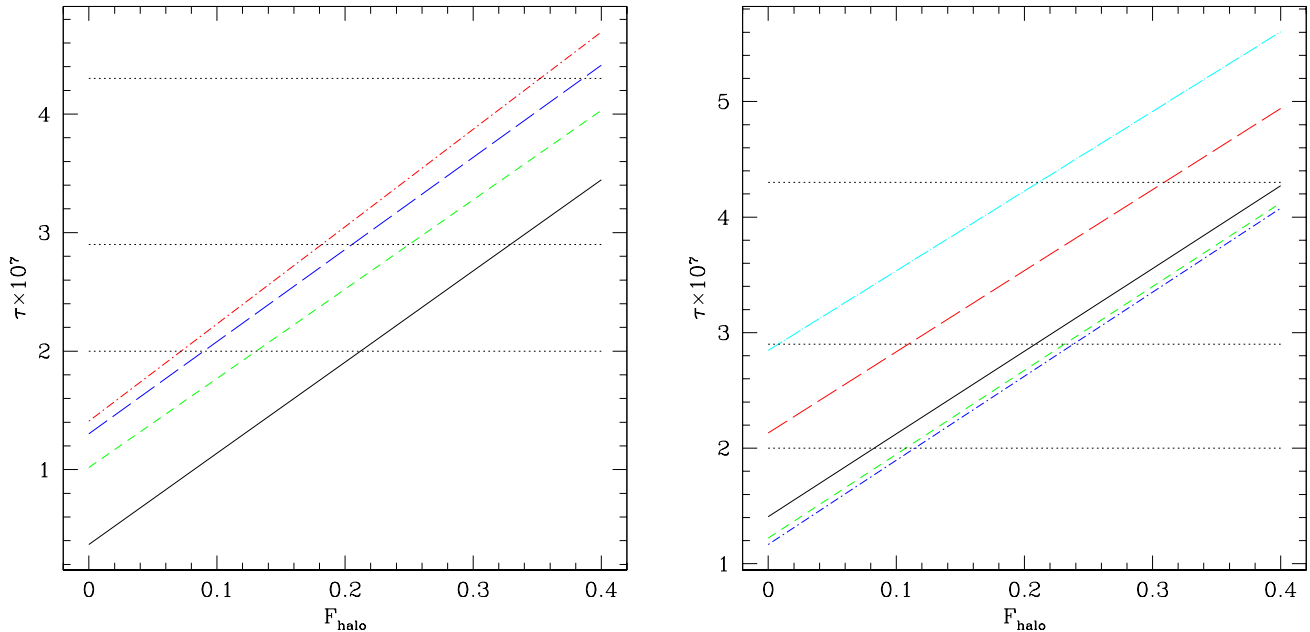


FIG. 12.— Left: microlensing optical depth as a function of MACHO fraction in the Galactic halo including MACHOs in LMC halo. The middle (upper, lower) horizontal dotted line show the observed microlensing ( $\pm 1\sigma$  confidence limits) from Alcock et al. (1997). Depth computed using the Kiraga & Paczyński  $\beta$  parameterization with  $\beta = -1$ . The four curves shows the predicted microlensing of the initial state (solid) and three successive pericenters (short-dash, long-dash, and dash-dot, respectively). Right: shows variation of microlensing optical depth as a function of disk inclination for the final pericenter shown at the left. The five curves show an inclination of 11.25, 22.5, 45, 67.5, and 78.25 degrees from bottom to top (short dash dot, short dash, solid, long dash, long dash dot, respectively).

First we assume no Galactic halo MACHOs; both source density  $\rho_s$  and deflector density  $\rho_d$  include only the stellar LMC distribution. This gives a total optical depth due to LMC self-lensing of  $1.4 \times 10^{-7}$  at the end of three LMC orbits (5.5 Gyr) in the simulation. This falls shy of the observed value,  $2.9_{-0.9}^{+1.4} \times 10^{-7}$ , by nearly two standard deviations although precise comparison is impossible since the simulation does not follow the entire LMC history. Nonetheless, self-lensing including the tidally evolved distribution is a significant contribution to the optical depth. The best fit value is  $F_{\text{halo}} \approx 0.21$  for the final orbit. If the Milky Way halo contains MACHOs, it is likely that the LMC halo also contains the same fraction. The LMC halo has one half of the total mass initially. In this case, the best fit is obtained for  $F_{\text{halo}} \approx 0.18$ . Figure 12 (left) shows the run of  $\tau$  with  $F_{\text{halo}}$  for this latter case.

The increase in the contribution to microlensing optical depth is dominated by the thickened disk rather than the lost stars in this simulation. Although mass is being lost continuously, the density profile near the disk is slowly changing after the first few orbits (as in Fig. 1 and reflected in Fig. 12 (left) for  $F_{\text{halo}} = 0$ ). However, this makes the self-lensing a strong function of disk inclination as shown in Figure 12 (right). For example, an inclination of 67.5, 78.25 degrees would imply  $F_{\text{halo}} = 0.11, 0.0$ , respectively. This is sensitivity is one-sided; decreasing the inclination below 45 degrees make little change in the  $\tau$  estimates.

In summary, the tidal disk heating makes a significant contribution to self-lensing. For no MACHOs,  $F_{\text{halo}} = 0$ , the optical depth of the tidally evolved disk is three times larger than the initial  $\text{sech}^2$  disk. This translates to a factor of two difference in the best estimate of  $F_{\text{halo}}$  (cf. Fig 1, left) and decreases the significance of rejecting the  $F_{\text{halo}} = 0$  hypothesis.

## 5. DISCUSSION

Although the physics of resonant heating and secular evolution applied here to thicken the disk and augment tidal stripping is well-understood and secure, several sources of wiggle room remain. First, the n-body simulations are technically difficult. There is no analytic method for constructing an equilibrium in a time-dependent tidal field so the initial model must come to a new equilibrium to start. The new virialized equilibrium has a weak rotating  $m = 1$  distortion that no doubt increases the heating rate although the disk heating during this initial period appears to be minimal. Because the simulation has been followed for nearly 5 Gyr and therefore many dynamical times, we took great care to estimate the rate of secular evolution due to intrinsic fluctuations. Both  $m = 1$  mode and fluctuation heating are smaller than the tidal effects. However, the heating from global excitation by noise or other sources can produce thickening and needs to be understood and treated with care by simulators.

A second uncertainty is the unknown initial conditions

for the LMC. The strongest evidence for the existence of some dark component is the weakly falling rotation curve indicated by globular clusters and planetary nebula (e.g. Schommer et al. 1992). This led to adopting an even mass split between the disk and halo components. Given the relatively short time for scale height growth why does the LMC appear to have a well-defined disk? A much more massive and an extended LMC halo would protect the luminous distribution from tidal stripping. On the other hand, such a halo is limited by self-lensing (assuming that it contains the same MACHOs attributable to the Galactic halo), constrained by the LMC rotation curve, would decrease the orbital decay time, and may be untenable given the observed SMC kinematics. In addition, such a halo is more readily stripped than the disk and the work done on the disk by the readjusting gravitational potential promotes heating in addition to the halo-disk coupling mentioned above.

Stripping is a natural consequence of the LMC–Milky Way interaction. A definitive failure to detect a stripped stellar component will necessitate a reevaluation of LMC structure. A speculative possibility is that a more massive LMC recently lost equilibrium in the Milky Way tidal field. The exposure of the disk to a significant tidal force might be recent. In such a scenario, the SMC most likely was a satellite of the larger primordial LMC and is now interacting directly with its luminous gas-rich disk. More generally, these dynamical mechanisms will affect all Magellanic-like systems and may help constrain their histories and determine the extent of their dark matter halos.

The current interest in MACHO detections and limits motivated some simple estimates of self-lensing by the LMC or by tidally-stripped LMC stars. Because the LMC orbit is fixed in the treatment here, the trail of unbound material at the end of the simulation is probably less extended than one might expect in Nature. Nonetheless, the self-lensing is dominated by material in the outer parts of the LMC or recently unbound and therefore this idealization seems unlikely to be significant. The simulation suggests an extension in front of the LMC due to material lost at or near pericenter that may be a possible explanation for the observed intervening stellar population toward the LMC reported by Zaritsky & Lin (1997).

## 6. SUMMARY

The major conclusions of this paper are as follows:

1. *The Milky Way is a significant evolutionary driver of LMC structure.* The time-dependent tidal forcing by the Milky Way will heat the LMC disk, producing extended rotating spheroid component.
2. *We find that the disk scale height increases at a rate of 70 pc/Gyr (cf. Fig 6).* The heating has several components. First, there is a direct resonant coupling between the time dependence of tidal forcing and the stellar orbits within the LMC disk. Second, the body torque from the Milky Way causes the LMC disk to precess. The interaction between the LMC halo and its precessing disk heats the disk. This is a *new* but important mechanism for heating the disks of satellites.
3. *The stellar velocity dispersion decreases due to disk heating.* The work done against the LMC gravitational potential decreases the depth of the potential well and the new quasi-equilibrium, although more extended, requires less velocity support. The sign of the effect follows from the virial theorem. Although a surprise to some, this effect has been well-documented for the evolution of star clusters.
4. *The mass loss rate is approximately  $3 \times 10^8 M_{\odot}$  per orbit or roughly 2% per orbit at the current time.* The fraction of halo loss to disk loss is roughly 3:1.
5. Because the heated, extended component is preferentially lost to tidal stripping, *the unbound stars will not be distributed like the Magellanic gas stream but in a diffuse distribution about the LMC.* This component may be a source of both microlensing sources and lenses and affect MACHO estimates. Overall, we estimate that the heated disk and tidally stripped component may make a significant contribution to gravitational microlensing.

I thank Neal Katz and Sergei Nikolaev for many useful discussions and Neal Katz and Eric Linder for comments on the manuscript. This work described here was supported in part by NSF AST-9529328 and NASA/JPL 961055.

## REFERENCES

- Aguilar, L., Hut, P., and Ostriker, J. P. 1988, *ApJ*, 335, 720.  
 Alcock, C., Allsman, R. A., Alves, D., Axelrod, T. S., Becker, A. C., Bennett, D. P., Cook, K. H., Freeman, K. C., Griest, K., Guern, J., Lehner, M. J., Marshall, S. L., Peterson, B. A., Pratt, M. R., Quinn, P. J., Rodgers, A. W., Stubbs, C. W., Sutherland, W., Welch, D. L., and The Macho Collaboration 1997, *ApJ*, 486, 697.  
 Bahcall, J. N. and Soniera, R. M. 1980, *ApJS*, 44(1), 73, Abstr. in 240, 374.  
 Binney, J. and Tremaine, S. 1987, *Galactic Dynamics*, Princeton University Press, Princeton, New Jersey.  
 Brueck, M. T. and Hawkins, M. R. S. 1983, *A&A*, 124, 216.  
 Chernoff, D. F., Kochanek, C. S., and Shapiro, S. L. 1986, *ApJ*, 309, 183.  
 Clutton-Brock, M. 1972, *Astrophys. Space. Sci.*, 16, 101.  
 Clutton-Brock, M. 1973, *Astrophys. Space. Sci.*, 23, 55.  
 Davies, R. D. and Wright, A. E. 1977, *MNRAS*, 180, 71.

- Fridman, A. M. and Polyachenko, V. L. 1984, *Physics of Gravitating Systems*, Vol. 2, p. 282, Springer-Verlag, New York.
- Fujimoto, M. and Sofue, Y. 1976, *A&A*, 47, 263.
- Gnedin, O. Y. and Ostriker, J. P. 1997, *ApJ*, 474, 223.
- Guhathakurta, P. and Reitzel, D. B. 1998, in *ASP Conf. Ser. 136: Galactic Halos*, p. 22.
- Henrard, J. 1982, *Cel. Mech.*, 27, 3.
- Hernquist, L. and Ostriker, J. P. 1992, *ApJ*, 386(2), 375.
- Irwin, M. J. 1991, in R. Haynes and D. Milne (eds.), *The Magellanic Clouds*, p. 453, Kluwer, Dordrecht.
- Jones, B. F., Klemola, A. R., and Lin, D. N. C. 1994, *AJ*, 107, 1333.
- Kalnajs, A. J. 1976, *ApJ*, 205, 745.
- King, I. R. 1966, *AJ*, 71(1), 64.
- Kinman, T. D., Stryker, L. L., Hesser, J. E., Graham, J. A., Walker, A. R., Hazen, M. L., and Nemeč, J. M. 1991, *PASP*, 103, 1279.
- Kiraga, M. and Paczyński, B. 1994, *ApJ*, 430, L101.
- Kochanek, C. S. 1996, *ApJ*, 457, 228.
- Kroupa, P. and Bastian, U. 1997, *New Astronomy*, 2, 77.
- Kunkel, W. E., Demers, S., Irwin, M. J., and Albert, L. 1997a, *ApJ*, 488, L129.
- Kunkel, W. E., Irwin, M. J., and Demers, S. 1997b, *A&AS*, 122, 463.
- Lee, H. M. and Ostriker, J. P. 1987, *ApJ*, 322(1), 123.
- Lin, D. N. C., Jones, B. F., and Klemola, A. R. 1995, *ApJ*, 439, 652.
- Lin, D. N. C. and Lynden-Bell, D. 1977, *MNRAS*, 181, 59.
- Lin, D. N. C. and Lynden-Bell, D. 1982, *MNRAS*, 198, 707.
- Meatheringham, S. J., Dopita, M. A., Ford, H. C., and Webster, B. L. 1988, *ApJ*, 327, 651.
- Murai, T. and Fujimoto, M. 1980, *PASJ*, 32, 581.
- Murai, T. and Fujimoto, M. 1986, *Ap&SS*, 119, 169.
- Murali, C. and Weinberg, M. D. 1997a, *MNRAS*, 288, 749.
- Murali, C. and Weinberg, M. D. 1997b, *MNRAS*, 291, 717.
- Nikolaev, S. and Weinberg, M. D. 1998, *BAAS*, 192, 5503.
- Olszewski, E. W., Suntzeff, N. B., and Mateo, M. 1996, *ARA&A*, 34, 511.
- Recillas-Cruz, E. 1982, *MNRAS*, 201, 473.
- Sanduleak, N. 1980, *PASP*, 92, 246.
- Schommer, R. A., Olszewski, E. W., Suntzeff, N. B., and Harris, H. C. 1992, *AJ*, 103, 447.
- Sellwood, J. A., Nelson, R. W., and Tremaine, S. 1998, *ApJ*, 506, 590.
- Silverman, B. W. 1986, *Density Estimation for Statistics and Data Analysis*, Chapman and Hall, London and New York.
- Tremaine, S. and Weinberg, M. D. 1984, *ApJ*, 282, L5.
- Vesperini, E. 1997, *MNRAS*, 287, 915.
- Wainscoat, R. J., M. Cohen, K. Volk, H. J. W., and Schwartz, D. E. 1992, *ApJS*, p. 111.
- Weinberg, M. D. 1994a, *AJ*, 108, 1398.
- Weinberg, M. D. 1994b, *AJ*, 108, 1403.
- Weinberg, M. D. 1994c, *AJ*, 108, 1414.
- Weinberg, M. D. 1994d, *ApJ*, 421, 481.
- Weinberg, M. D. 1995, *ApJL*, 455, L31.
- Weinberg, M. D. 1996, *ApJ*, 470, 715.
- Weinberg, M. D. 1997, *ApJ*, 478, 435.
- Weinberg, M. D. 1998, *MNRAS*, 299, 499.
- Weinberg, M. D. 1999, *AJ*, 117, 629.
- Wu, X. P. 1994, *ApJ*, 435, 66.
- Zaritsky, D. and Lin, D. 1997, *AJ*, 114, 2545.

## APPENDIX

### LMC PARAMETERS

#### *The LMC tidal radius and mass*

Star count maps of the outer LMC (e.g. Irwin 1991) show an extended distribution with a fairly sharp edge, typical of a tidally truncated system. To get an independent measurement using 2MASS star counts, we selected 12 subfields  $0.5^\circ \times 0.5^\circ$  in size which probe the LMC halo at the projected radii of  $2^\circ - 5^\circ$  from the LMC center ( $l_{II} = 280.5^\circ$ ,  $b_{II} = -32.9^\circ$ ). The counts were fit to Gaussian and power-law spherical models,  $\rho \propto e^{-r^2/2a^2}$  and  $\rho \propto (1+r^2/a^2)^{-\gamma}$ , using a maximum likelihood procedure. The simple analytic forms for these profiles make the likelihood computation feasible. To estimate the mass of the LMC, we fit these analytic profiles by King models to estimate the tidal radius:

$$M_{LMC} = \left( \frac{r_t}{R_{LMC}} \right)^3 2M_{MW}, \quad (\text{A1})$$

where  $R_{LMC}$  is the distance to the LMC and  $M_{MW} = 5 \times 10^{11} M_\odot$  is the mass of the Milky Way. This is a total mass estimate, including both the halo and the disk mass.

This procedure will underestimate the mass for two reasons. First, simulations suggest that the observed  $r_t$  is 75%–80% of the dynamical critical point. Second, a tidally-limited object is likely to be elongated toward the Galactic center and therefore roughly along the line of sight. For a centrally-concentrated object, the axis ratio is  $a/c = 1.5$ . The first correction yields a factor of  $(10/8)^3 \approx 2$ . The second increases the enclosed volume by roughly 3/2 but whether or not this should be included depends on orientation. A reasonable correction factor is then between 2 and 3 and we conservatively choose the former. The parameters of the ‘best fit’ models are  $a = 2.6, 2.8$  for the Gaussian and power-law model with  $\gamma = 2$ , respectively. For both cases, the lower mass limit is  $1 \times 10^{10} M_\odot$  with a best estimate of  $2 \times 10^{10} M_\odot$ . An in-depth presentation of these results is in preparation.

As an independent check, we made a naive estimate of the mass of the LMC from the analysis of the halo population using the star counts in our fields. Most of the sources observed by 2MASS are M-giants with the absolute magnitude in K-band  $K < -4^m$  (for the distance to the LMC of 50 kpc and 2MASS  $K_s$ -band  $SNR = 10$  flux limit of  $14.3^m$ ). Assuming that these M giants are representative of an intermediate age population with the extended distribution derived above, we may estimate the total stellar mass using an infrared luminosity function. For this purpose, we adopt the Galactic luminosity function in Wainscoat et al. (1992). Integrating over the luminosity function with a standard luminosity-mass relation results in stellar mass of  $\approx 4 \times 10^9 M_\odot$ , which is consistent with these estimates.

Schommer et al. (1992) summarizes the derived rotation curve for clusters, planetary nebulae and HI including the Meatheringham et al. results (see Schommer et al. Fig. 8). Using a luminosity function derived for an exponential disk and typical velocity dispersion in halo with a flat rotation curve, one finds that the circular velocity  $V_c$  is roughly 20–30% larger than the rotation value  $V_o$ . For a rotation curve with  $V_o \approx 75$  km/s, one finds a mass within 10.8 kpc of  $M \gtrsim 2 \times 10^{10} M_\odot$  which is nicely consistent with the tidal radius estimate. See Schommer et al. for more extensive discussion of these arguments.

## COMPUTATIONAL NOTES

### *Grid-based Boltzmann solution*

The evolution of a perturbed equilibrium can be explored with a time-dependent perturbation theory (e.g. Weinberg 1994b, Murali & Weinberg 1997a). The physics behind this approach is as follows. The period of the LMC orbit is longer than the periods of many of the stellar orbits within the cloud and such orbits are adiabatically invariant to the time-dependent tidal forcing. However, in cases where the frequencies of the stellar orbit are commensurate with the forcing frequencies, the resulting degeneracy breaks the adiabatic invariant. The change in the gravitational potential causes the resonance to sweep through phase space as described in §3.1 and the direction of the passage determines the effect of the resonance on the conserved quantities. The net effect on the gravitational potential depends on the scale of the inhomogeneity in the phase-space distribution. The evolution equations, therefore, take the form of a collisional Boltzmann equation with the right hand side depending on a gradient of phase space. Numerically, we approximate the solution of this equation by a two step process:

1. Update the phase-space distribution function in a fixed potential using the finite-difference representation for the evolution term on the right hand side. This term can be written in flux form as described below and therefore conserves density over one step.
2. Hold the distribution function fixed as a function of actions and solve for a new equilibrium. For ease of solution, the potential is assumed to have spherical symmetry while the distribution itself may be generally axisymmetric (e.g.  $f = f(E, L, L_z)$ ).

### *Resonant heating rates*

The linearized Boltzmann equation is a linear partial differential equation in seven variables. Using action-angle variables, we can separate the equation and employ standard distribution functions constructed according to Jeans' theorem (Binney & Tremaine 1987). The explicit form of the linearized Boltzmann equation is

$$\frac{\partial f_1}{\partial t} + \frac{\partial f_1}{\partial \mathbf{w}} \frac{\partial H_0}{\partial \mathbf{I}} - \frac{\partial f_0}{\partial \mathbf{I}} \frac{\partial H_1}{\partial \mathbf{w}} = 0, \quad (\text{B1})$$

where  $\mathbf{w}$  is the vector of angles, and  $\mathbf{I}$  are the conjugate actions. The quantities  $f_0$  and  $H_0$  depend on the actions alone. Making the assumption that the tidal force from the Galaxy is small, the perturbation may be separated into phase-space and time components,  $H_1 = \eta(\mathbf{r})g(t)$ , expanded in a Fourier series in action-angle variables (e.g. Tremaine & Weinberg 1984). Each term  $f_{1\mathbf{l}}$  in the Fourier series is the solution of the following differential equation:

$$\frac{\partial f_{1\mathbf{l}}}{\partial t} + (i\mathbf{l} \cdot \Omega)\mathbf{f}_{1\mathbf{l}} = i\mathbf{l} \cdot \frac{\partial \mathbf{f}_0}{\partial \mathbf{I}} \mathbf{V}_1(\mathbf{I})\mathbf{g}(t) \equiv i\mathbf{l} \cdot \frac{\partial \mathbf{f}_0}{\partial \mathbf{I}} \mathbf{H}_{1\mathbf{l}}, \quad (\text{B2})$$

where  $\Omega = \partial \mathbf{H}_0 / \partial \mathbf{I}$  and

$$V_1(\mathbf{I}) = \frac{1}{(2\pi)^3} \int_{-\pi}^{\pi} \eta(\mathbf{r}) e^{-i\mathbf{l} \cdot \mathbf{w}} \mathbf{d}^3 \mathbf{w}. \quad (\text{B3})$$

The quantity  $\mathbf{l}$  is a vector of integers whose rank is the number of degrees of freedom; e.g. for the three dimensional problems considered here,  $\mathbf{l} = (l_1, l_2, l_3)$ . In practice, we usually confine our perturbation to a particular set of spherical harmonics or cylindrical harmonics which restricts two out of three to a finite set (see Tremaine & Weinberg 1984 for details).

The rate of change in energy or action arising from the perturbation follows from Hamilton's equations and is

$$\begin{aligned} \dot{E} &= \sum_{\mathbf{l}=-\infty}^{\infty} i\mathbf{l} \cdot \Omega \mathbf{H}_{1-\mathbf{l}} \mathbf{f}_{\mathbf{l}} \\ \dot{I}_j &= \sum_{\mathbf{l}=-\infty}^{\infty} i l_j H_{1-\mathbf{l}} \mathbf{f}_{\mathbf{l}}. \end{aligned} \quad (\text{B4})$$

For periodic perturbations, the time dependent amplitude may be represented by a Fourier series,

$$g(t) = \sum_{n=-\infty}^{\infty} a_n e^{in\omega t}. \quad (\text{B5})$$

With this form for  $g(t)$ , equation (B2) may be solved for the perturbed distribution function by Laplace transform. Finally, phase averaging the quantities in equations (B4) yields the following time-asymptotic rates:

$$\langle \dot{E} \rangle = -8\pi^4 \sum_{\mathbf{l}=-\infty}^{\infty} (\mathbf{l} \cdot \boldsymbol{\Omega}) (\mathbf{l} \cdot \frac{\partial \mathbf{f}_0}{\partial \mathbf{I}}) |\mathbf{V}_1|^2 \sum_{\mathbf{n}=-\infty}^{\infty} |\mathbf{a}_n|^2 \delta(\mathbf{n}\omega - \mathbf{l} \cdot \boldsymbol{\Omega}). \quad (\text{B6})$$

$$\langle \dot{I}_j \rangle = -8\pi^4 \sum_{\mathbf{l}=-\infty}^{\infty} l_j (\mathbf{l} \cdot \frac{\partial f_0}{\partial \mathbf{I}}) |\mathbf{V}_1|^2 \sum_{n=-\infty}^{\infty} |a_n|^2 \delta(n\omega - \mathbf{l} \cdot \boldsymbol{\Omega}). \quad (\text{B7})$$

Murali & Weinberg (1997a) show that this expansion, continued to the next order, results in an equation for the change in distribution function in terms of these rates which takes the form:

$$\langle \dot{f}_2 \rangle \propto \frac{\partial}{\partial \mathbf{I}} \cdot \langle \dot{\mathbf{I}} \rangle \quad (\text{B8})$$

which may be solved by standard flux-conserving finite-difference methods.